6

# Synthesis, Microstructure and Properties of High-Strength Porous Ceramics

Changqing Hong, Xinghong Zhang,
Jiecai Han, Songhe Meng and Shanyi Du
*Center for Composite Materials and Structure, Harbin Institute of Technology, Harbin, PR China*

## 1. Introduction

Porous ceramics containing tailored porosity exhibit special properties and features that usually cannot be achieved by their conventional dense counterparts. Thus, porous ceramics find nowadays many applications as final products and in several technological processes. Porous ceramics are of significant interest due to their wide applications in high-temperature filters, thermal gas separation, lightweight structural components and thermal structural materials (Peng, H.X et al, 2000; Corbin, S. F and Apte, P. S 1999; Fukasawa, T et al; 2001).

To meet these requirements, various fabricating methods are adopted to produce highly porous ceramics. These processing methods include the replication of polymer foams by ceramic dip coating, the foaming of aqueous ceramic powder suspensions, the pyrolysis of preceramic precursors, partial sintering by pressureless sintering, and the firing of ceramic powder compacts with pore-forming fugitive phases (Kamal, M. M et al 2006; Amir, M. and Rohwer, K, 2007; Hong, C. Q et al 2007; Dale, H &David, J. G, 1995; Oh, S.-T et al, 2001; Deng, Z.-Y et al,2002; Deng, Z. Y et al,2001)

Often for porous ceramics used in high temperature environment, they require high temperature melting point, high mechanical strength, low thermal conductivity, open pore structure and special pore distribution. For example, with the development of modern spaceflight technology, active cooling is becoming a very efficient mode of thermal protection for high heat load structures. In active cooling, coolant is usually injected or infiltrated into a porous ceramic, and then transpirated to reduce the bulk temperature for thermal protection (Hong, C.Q et al 2007). The components used for active cooling are always subjected to severe environments with ultra-high temperature, high-pressure, and usually supersonic velocity. Therefore, the porous ceramic in active cooling must have high melting point, moderate framework strength, and reasonable pore distribution regularity.

The properties for porous ceramics can be tailored for specific environmental application by controlling the composition and microstructure of the porous ceramic. Changes in open and closed porosity, pore size distribution and pore morphology can have a major effect on a material's properties. All of these microstructural features are in turn highly influenced by the processing route used for the production of the porous material. For the mechanical properties, porous ceramics are determined by their structure parameters, such as porosity, pore size, and pore structure (Deville, S et al, 2006; Gough, J. E et al, 2004). Additionally, the

microstructure of the solid phase related to neck growth and solid phase continuity strongly affect the mechanical properties. Several important issues regarding the neck growth between touching particles by surface diffusion and volume diffusion can significantly increase the mechanical properties with minimal increase in density. The microstructure in porous ceramics can be controlled not only by adjusting the particle size and shape of the initial powders, but also by the sintering process (Studart, A. R et al, 2006; Koh, Y. H et al,2006; Schmidt, H et al, 2001)

The objective of this chapter is to adopt partial/pressureless sintering and freeze-casting routes for the preparation of high-strength porous titanium diboride ($TiB_2$) and porous $ZrO_2$ ceramics, with particular emphasis on the processing–microstructure–property relations inherent to each process.

## 2. Production of porous diboride titanium

### 2.1 Porous $TiB_2$

$TiB_2$ has been regarded as promising candidate materials for structural applications for its unique combination of higher melting point, good strength, good thermal stability, and corrosion resistance.

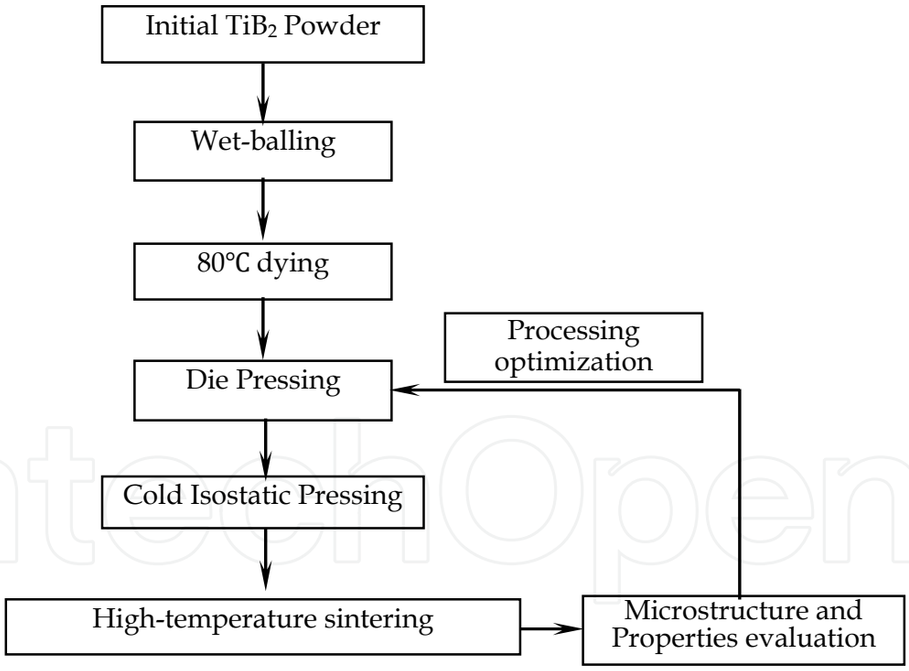


Fig. 1. Technologic flow for preparing porous $TiB_2$ ceramic

The constituent materials used in this study were $TiB_2$ powder (produced by Northwest Institute for Non-Ferrous Metal Research, Xi'an, People's Republic of China) with particle mean size of 2–4μm and purity of 98 per cent. In order to reduce the agglomerated $TiB_2$ powder to single particles, $TiB_2$ starting powder was milled by the wet-milling method for 4 h in a plastic bottle with agate balls and acetone as media. The resultant slurry was dried in a vacuum evaporator. The dried powder was screened through an 80-mesh screen. After

that, the powder was prepressed in the cylindrical type mould with the L/D ratio of 1:2 and 30mm diameter under a uniaxial pressure of 10MPa. Then they were compacted by a cold isostatic press (CIP) machine at room temperature. The CIP pressures were 50, 100, and 200MPa, and they were maintained for 200s. The green-compacted billets were sintered in a furnace, in a vacuum atmosphere, at a heating rate of 10 °C/min. All specimens were held at the sintering temperature for 30 min and then cooled to room temperature at the same rate of 10 °C/min. Different sintering temperatures in a range of 1650–2000 °C were used in the present experiment to produce specimens of different porosities.

### 2.2 Microstructure

Fig.2 shows the dependence of relative density on sintering temperature of $TiB_2$ porous ceramic. It can be seen that the relative density increases as the sintering temperature increases. For the sake of the lower density of the formed green compacts, the billets with low initial pressure required a higher temperature to reach the same density when compared with the high initial pressure.

Fig 3(a) and (b) show the macro-morphology of sintered and machined porous $TiB_2$ samples. The sintered sample fundamentally kept its shape and no macroscopic defects were found after machining.

Fig.4 shows the microstructures of porous $TiB_2$ specimens sintered from different compacts at 2000 °C. Because of the low sintering temperature, the original morphology of $TiB_2$ grains produced by the compaction can be seen clearly. A number of voids and small flaws existed in the specimen, due to a loose connection between the $TiB_2$ grains. However, these voids and small flaws were reduced greatly with the increasing temperature, indicating a better connection between the $TiB_2$ grains. The weak interface strength in porous $TiB_2$ ceramic sintered from lower pressured compacts originated from the poor connections of $TiB_2$ grains (Fig. 4(a)). However, the highly packed regions densified faster than the less-dense regions, as shown in Fig. 4(b) and (c), suggesting that the surface diffusion is enhanced and promotes the preferential neck growth with certain increase in density.

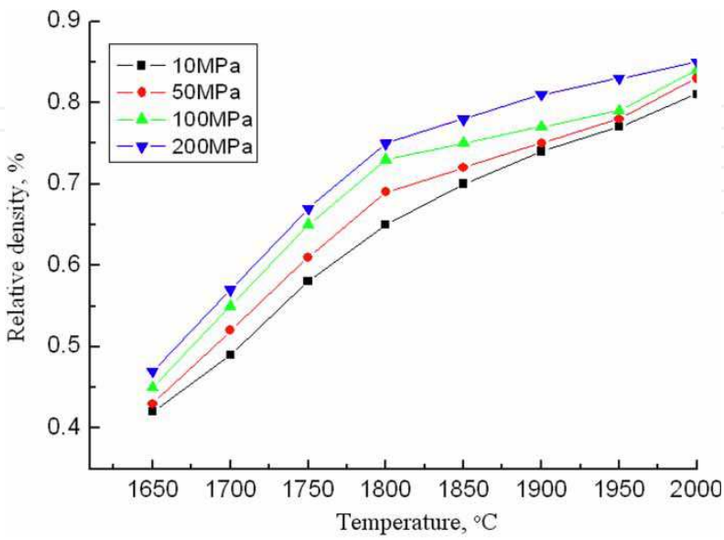


Fig. 2. Dependence of relative density on sintering temperature of TiB2 porous ceramic

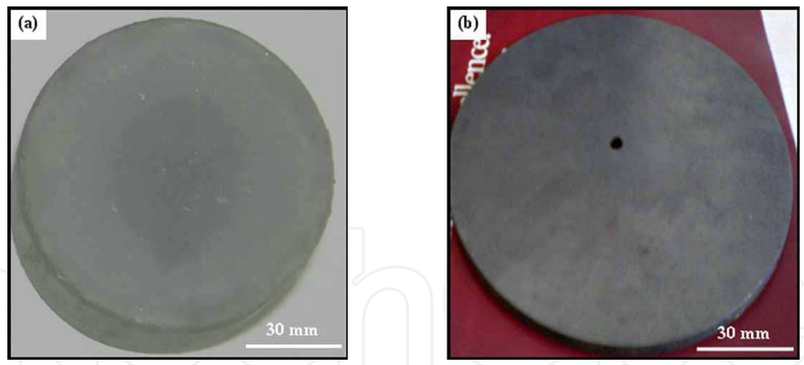


(a) sintered sample (b) machined sample

Fig. 3. Macro-morphology of porous TiB2 sintered at 2000 °C,

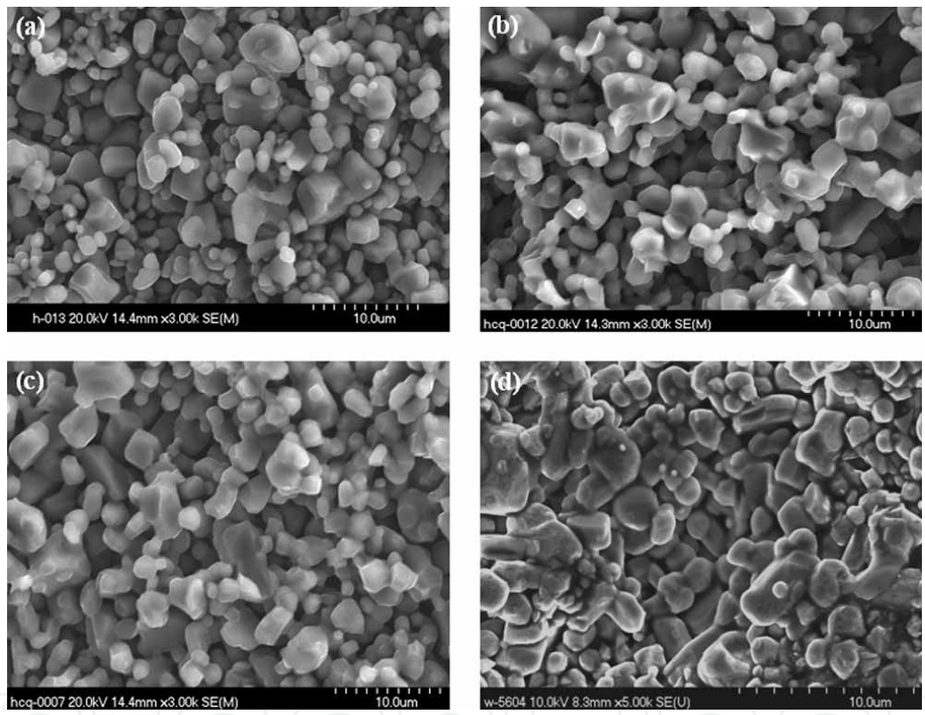


Fig. 4. SEM micrographs of TiB2 porous ceramics sintered at 2000 °C with different initial compacted pressures: (a) 10MPa; (b) 50MPa; (c) 100MPa; (d) 200MPa

Fig. 5 shows the microstructure of the specimens (initial pressures of 100MPa) sintered at 1750, 1800, 1850, and 1950 °C. Clearly, the size of the pores between grains decreases with the increase of sintering temperature, which is consistent with the variation of relative density in Fig. 2. Moreover, it can be observed (Fig. 5) that the grain size does not increase dramatically with sintering temperature. Another noteworthy observation in Fig.5(d) is the formation of well developed necks between grains, which should be responsible for the improved mechanical strength.

Because $TiB_2$ belongs to the covalently bonded solids, the intrinsic diffusivity is very low and therefore the Peierl's stress is high for the movement of dislocations. The preferential neck growth in mass transfer was affected by evaporation–condensation and surface

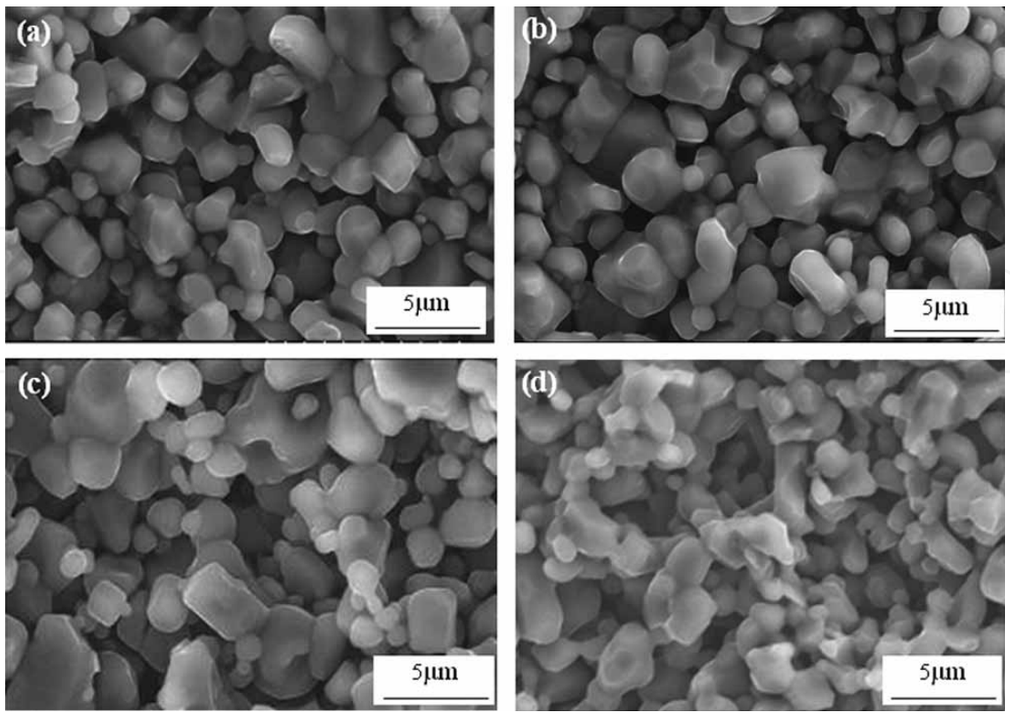


Fig. 5. SEM micrographs of TiB2 porous ceramics sintered with initial compacted pressure of 100MPa at different sintering temperatures: (a) 1750 °C; (b) 1800 °C; (c) 1850 °C; (d) 1950°C

diffusion. According to Bhaumik (Bhaumik, S. K et al, 2001) and Wang (Wang and Fu, 2002), the dominant sintering mechanism for$TiB_2$ is surface diffusion and subsidiary volume diffusion at such an experimental sintering condition. The surface diffusion does not result in shrinkage but in the formation of solid bonds between adjacent particles. As the temperature increases, the enhanced neck size of $TiB_2$ grains was enhanced and bridges between particles were well developed (Fig. 5(d)). The promoted neck formation between particles by surface diffusion gives rise to such microstructural feature.

### 2.3 Mechanical properties

Figures 6 and 7 show the dependence of bending strength and fracture toughness on the relative density of porous$TiB_2$ ceramic sintered from the compacts under different pressures. In general, the mechanical properties of porous $TiB_2$ followed the expected trend, i.e. fracture strength and toughness increased with increasing relative density. This indicated that high compaction pressures improve the mechanical properties of porous $TiB_2$ ceramics. As shown in Fig. 5, e.g. the strengths (with initial pressure of 10 and 100MPa, respectively) having 80 per cent relative density retain high strength of about 175 and 215MPa, respectively. The high strength must be related to the growth of the interparticle contacts (neck growth) by surface diffusion, which will be discussed in next section.

The fracture toughness of the porous $TiB_2$ ceramic shows a similar trend as the flexural strength, as demonstrated in Fig. 7. The fracture toughness of porous $TiB_2$ ranged from 0.5 to 2.4MPa$m^{0.5}$ for initial pressure of 10MPa; while the fracture toughness increased from 0.8 to 3.5MPa$m^{0.5}$for initial pressure of 100MPa, indicating initial compacted pressure and the

relative density (induced by sintering temperature) have an important influence on the mechanical properties.

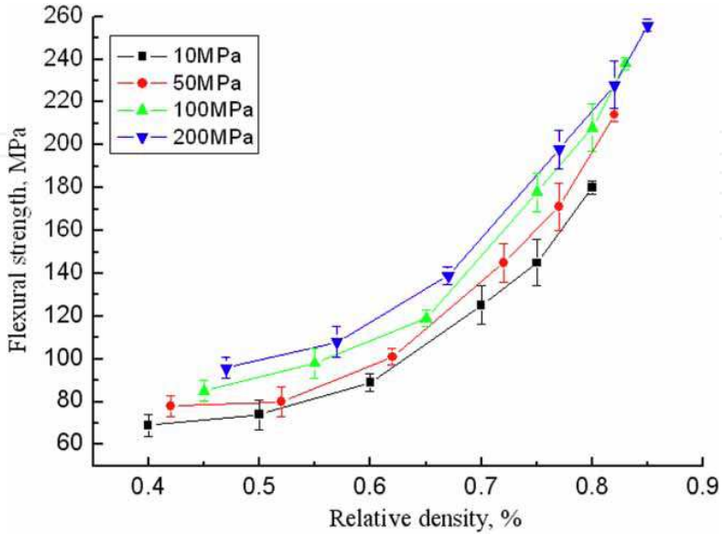


Fig. 6. Dependence of flexural strength on relative density of TiB2 porous ceramic

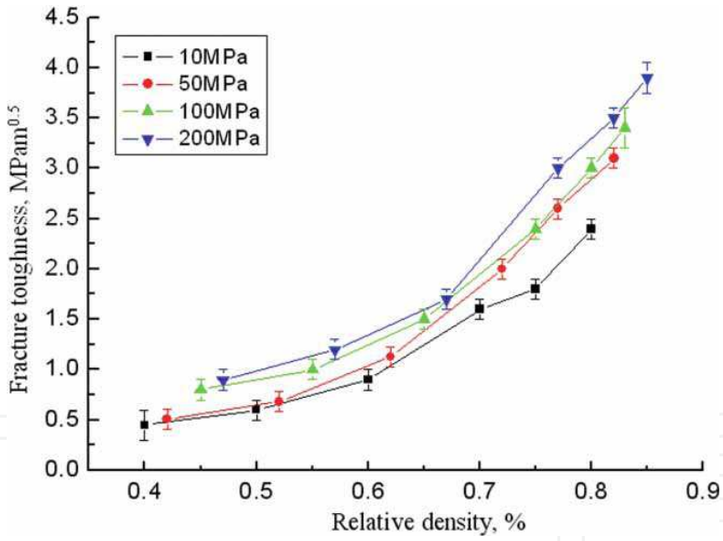


Fig. 7. Dependence of fracture toughness on relative density of TiB2 porous ceramic

### 2.4 Mechanical mechanism

Generally, high mechanical strength is desirable simultaneously with high porosity for almost all applications of porous ceramics. The relationship between strength and porosity has been investigated by many researchers, and a number of models have been proposed to explain the strength–porosity behaviors. Based on the assumption that the fracture strength of porous ceramics is determined by the minimum solid area, one of the simplest expressions was given by Rice (Rice, R. W et al, 1993)

$$\sigma = \sigma_0 \exp(-bP) \quad (1)$$

where $\sigma_0$ is the strength of a non-porous structure, $\sigma$ is the strength of the porous structure at a porosity $P$, and $b$ is a constant that is dependent on the pore characteristics. This expression indicates that strength will increase with decreasing of porosity, and this seems to agree with our results. However, from Fig. 6, it can be seen that the fracture strength increased with the increasing of initial pressure for a certain relative density. This reveals that the strength for porous ceramics is not only controlled by pore volume content but also influenced by special microstructure, sintered neck bonding or neck growth. Actually for highly porous materials, the stress concentration associated with pores no longer defines the mechanical behavior, as the effects due to surface defects are negligible. Hence, the strength values obtained in this study may have no dependency on effective pore volume. It is also noteworthy to mention that the enhanced strength of porous

$TiB_2$ must be related to the growth of the interparticle contact (neck growth) by surface diffusion, in the initial stage of sintering. This increase in strength with minimum densification is a significant factor for the mechanical behaviour of porous ceramics. The strength improvements are also afforded by control of the sintering mechanism and the microstructural homogeneity.

Extensive investigations revealed that mechanical properties of porous ceramics are related to the theory of minimum solid contact area (MSA) [Rice, R. W et al, 1993] when no special reinforcing mechanisms exist. If the particle stacking is a cubic array and the particles are spherical, MSA is the necking area between the particles, i.e. the grain bonding area. If the particle stacking is not the cubic array, the grain bonding area is a representation of MSA. For this study, as the fracture mode of porous $TiB_2$ ceramics is intergranular (Fig. 8), the bonding interface is the place of greatest stress concentration. Moreover, the shape of $TiB_2$ grains is equiaxed and no special reinforcing mechanisms can be found in this material. The weak interface strength in porous $TiB_2$ ceramics sintered from an initial pressure of 10 and 50MPa originates from the $TiB_2$ fragments and their poor connections (Figs 4(a) and (b)). Because highly packed regions (under higher compacted pressure) densified faster than the less-dense regions (under lower compacted pressure), as shown in Figs 4(c) and (d), where the $TiB_2$ grains on neck regions show poor connections. Comparably the $TiB_2$ grains from an initial pressure of 100 and 200MPa reveal good necking bonding and connection.

At the initial stage of densification, the sintering shrinkage is small and the difference in boundary defects for different compacts is small. The resultant interface bonding and mechanical properties of porous $TiB_2$ display limited differences between the compact with relatively lowpressures. As densification progresses, the sintering shrinkage increases and the difference in boundary defects and the resultant interface bonding increase. Therefore, mechanical property differences increase with increasing relative density according to the MSA analysis.

Fracture toughness is a property that enables the materials resist to the propagating of cracks. However, for a porous ceramic, the crack tip field distribution differs from the dense ceramic material. On one hand, the crack tip becomes blunt as a crack meets an open pore in a porous ceramic. Deng *et al.*(Deng, Z.-Y et al, 2002) had demonstrated the reinforcing effect of crack-tip blunting in porous SiC ceramics. This decreases the stress-concentration at the crack tip and increases the external load to propagate the crack so that the fracture

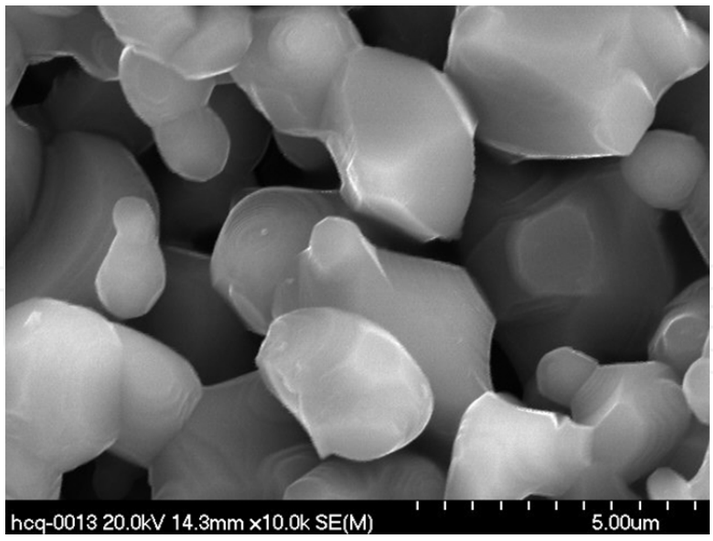


Fig. 8. Magnified fracture morphology of porous TiB2 sintered at 2000°C with initial pressure of 100 MPa

toughness increases (as shown in Fig.9). On the other hand, as discussed above, the higher initial compacted pressure and higher sintering temperature will enhance the neck growth and grain-boundary strength, which contributes to the increase of fracture toughness.

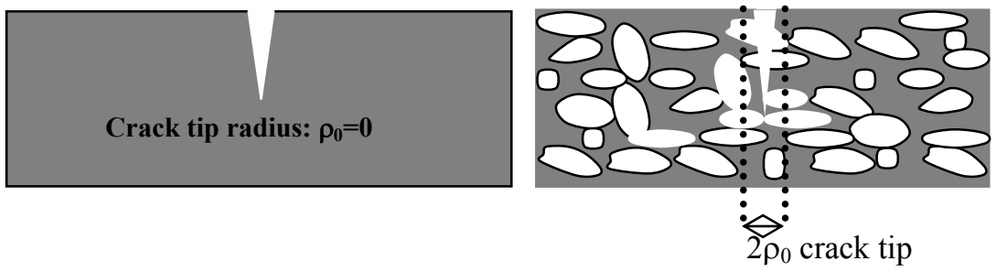


Fig. 9. Sharp and blunt crack tip of two types of materials

## 3. Production of porous zirconia

### 3.1 Porous $ZrO_2$

Commercially available yttria-stablized zirconia doped with 5 mol%$Y_2O_3$ (0.4μm, Fanmeiya powders Co. Ltd., Jiangxi, China) was used as the ceramic framework. Camphene ($C_{10}H_{16}$) (95% purity, Guangzhou Huangpu Chemical Factory, Guangzhou, China) was used as the freezing vehicle without any further purification. In addition, Texaphor 963 (Guangzhou Haichuan Co. Ltd., Guangzhou, China) was used as dispersant (density at 25 $^oC$ of 0.89-0.91 $gcm^{-3}$). The dispersant concentration was 3 wt.% of the $ZrO_2$ powder for all 10, 15 and 20 vol.% of solid loadings.

The first part of the manufacturing process involved the slurry preparation. This was achieved by melting the camphene at a temperature of 60 $^oC$ on a heating plate to create a clear and fluid vehicle. The dispersant concentration was 5 wt.% of $ZrO_2$ powder for all solid

loadings. The $ZrO_2$ powder was then added in quantities of 10, 15and 20 vol.%. The slurry was stirred via the use of a motor and stirrer with a cap on the top to prevent any camphene vapour escaping. Zirconia/camphene/dispersant slurries with various Zirconia contents (quantities of 10, 15 and 20 vol%) were prepared by ball-milling at 60oC for 20h, before pouring into silicone rubber die for freezing; the moulds were 42 mm in internal diameter and 80 mm in height.

The samples were left to cool at ice-water environment (0 $^{o}$C) for 30 min. The detailed above sketch of the test setup is shown in Fig.10 (a). Meanwhile some samples were cooled at liquid nitrogen environment (-196$^{o}$C) for the same length of time to study the effect of cooling rate on the solidification characteristics, which can be seen from Fig.10 (b). After solidification, the green body was removed from the moulds and left to sublime (optimized to 24 h) at room temperature in order to remove the camphene entirely and achieve a highly porous structure. Following sublimation, sintering of the green body at 1400-1550 $^{o}$C enabled the densification of the samples and concomitant improvements in mechanical

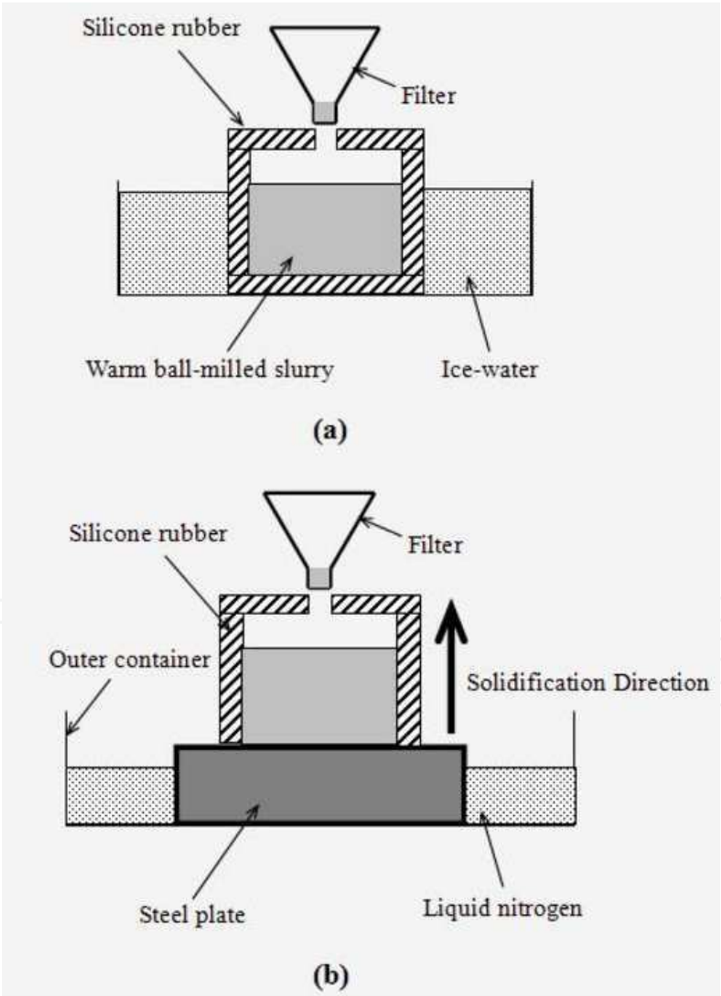


Fig. 10. A sketch of freezing assembly for fabricating cast body (a) in ice-water environment; (b) in liquid nitrogen cooling environment

strength. The sintering regime entailed heating the samples at 0.5 $^{o}$C/min up to 600 $^{o}$C followed by 1 h of dwell time. They were then heated at 1 oC/min up to final sintering temperature and held at this temperature for 2 h, prior to cool down to room temperature at the same rate of 20 $^{o}$C /min.

### 3.2 Camphene solidification observations

The solidification phenomenon of the mixed slurry was investigated so as to acquire an understanding of the characteristics of pore and dendrite formation. Fig. 12(a) shows the development of long and straight dendritic branches near the marginal corner along the freezing plane, which runs towards the left corner (as shown by the arrow). Since the temperature gradient at the marginal region decreases fast, the camphene crystals grow dendritically in certain crystallographic directions. When the solidification was completed, a unique phase separated structure was produced, in which aligned camphene dendrites with a well-defined morphology surrounded by $ZrO_2$ particle networks were formed.

Fig. 12(b) shows the interconnectivity of the camphene branches near the central region of the slide where the temperature gradient was sufficiently high to stimulate secondary dendritic formation, and many short elongated camphene dendrites were formed randomly. A typical dendritic growth of camphene as well as $ZrO_2$ particle rejection of the warm slurry is shown in Fig.11.

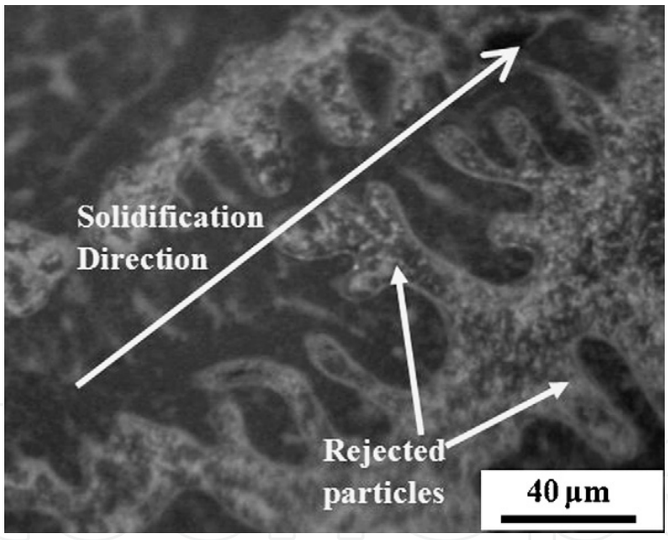


Fig. 11. Typical dendritic growth and particle rejection for camphene-based slurry

It can be seen that the development of dendritic branches along the freezing plane, which, in the image, runs towards the top right corner. The particles are not only pushed along ahead of the advancing macroscopic solidification front composed of tips of growing dendrites, but are also connected on the spot after being rejected by dendrite arms. The macro-morphology in the center region of the slide where no camphene dendrites were found (shown in Fig.12(c)). Due to the low temperature gradient in the center region (since both top and bottom slide glass were covered by silicone rubber insulation), some of the dendrite side arms might be melted off and then act as seeds for new dendrites, resulting in the formation of equiaxed pore structures. The above observations reveal the morphology of the

dendrites that are produced during freezing of the camphene and the important role of the heat transfer gradient on determining the final shape and orientation.

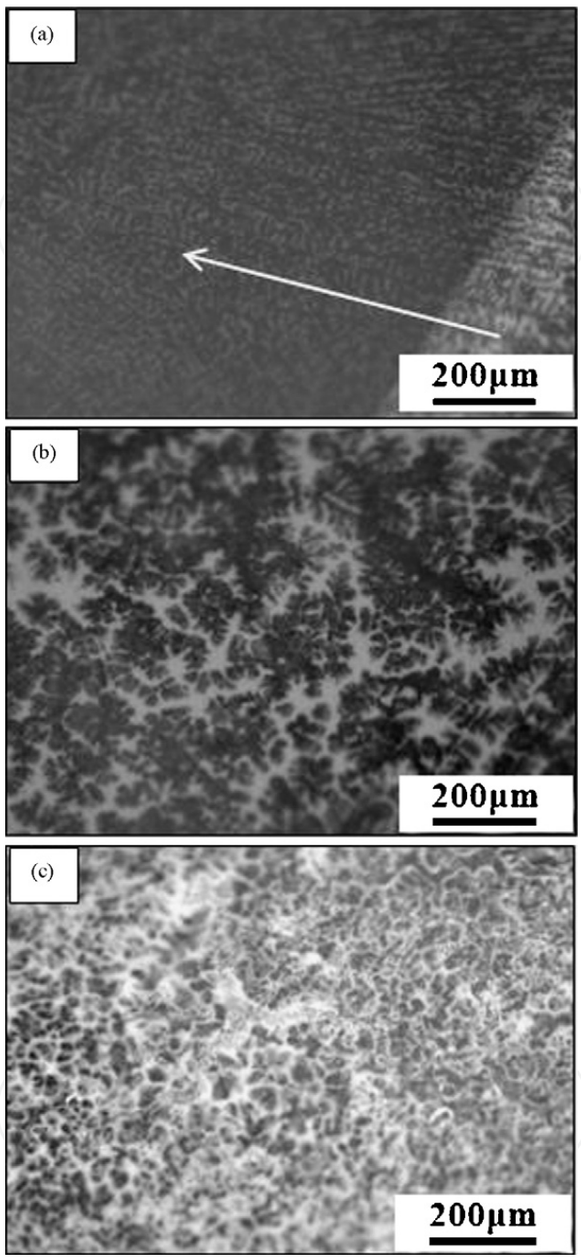


Fig. 12. Optical micrographs of the camphene dendritic growth during solidification (a) aligned camphene growth (shown by the arrow); (b) typical dendritic growth; (c) equiaxed camphene morphology.

### 3.3 Unidirectional solidification

Because the sintered pore structure form as replicas of camphene dendrites, unidirectional solidification was tried to control the growth direction of the camphene dendrites. A special

mold composed of a steel bottom plate and a silicone rubber die on it was prepared to create a cylindrical cavity. Warm ball-milled $ZrO_2$ slurry of 60 °C with 15 vol.% solid content was poured at room temperature into the prewarmed mold having almost the same temperature as the slurry. Just after casting, liquid nitrogen was poured into the outer container to cool only the steel bottom plate so that the solidification of the camphene-based slurry would occur unidirectionally from the bottom towards the top in the mold. The solidification was completed in about 3 min, and then the cast body was dried in an ambient atmosphere for 30h.

Sintered samples generated with solid loadings of 15 vol.% were analyzed by SEM. The SEM micrographs (Fig. 13(a) and (b)) showed that the pores tend to align in the direction of freezing, indicating the possibility of controlling pore orientation by controlling parameters such as the heat transfer gradient and direction of freezing. Since the chilled mold was suddenly cooled with liquid nitrogen about −160 °C, the camphene rapidly cooled below its solidification temperature, and thus many nuclei of the camphene then form on the mold wall and begin to grow into the warm slurry. Under these conditions, most of the nuclei do not have a preferential orientation that corresponds to the direction of the heat conduction. Therefore, these camphene crystals cannot overgrow dendritically, and these results in the formation of long straight channels in the sintered body (see Fig. 11).

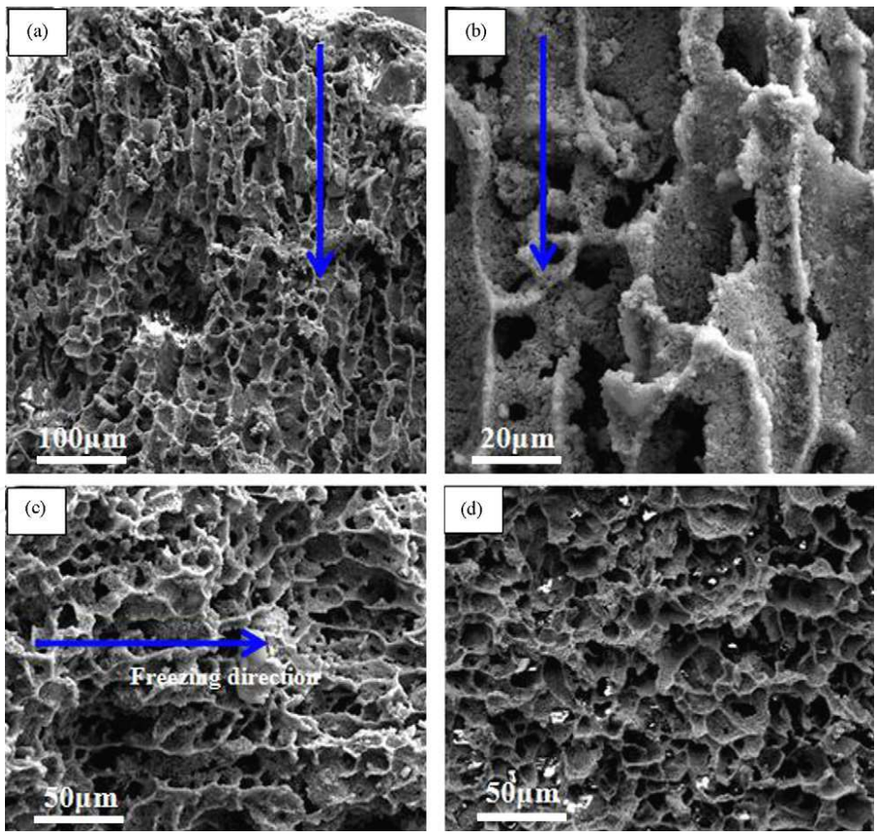


Fig. 13. (a) Pore alignment in the direction of freezing; (b) magnified microstructure in Fig. 2(a); (c) dendritic pore distribution beyond the die wall; (d) equiaxed pore morphology in the center of sintered sample

Beyond the above region, the temperature gradient near the die wall decreases and the camphene crystals began to grow dendritically in certain crystallographic directions. Those crystals with a preferential orientation close to the direction of heat flow, i.e., parallel to the mold wall, grow faster and can lead to their secondary dendritic formation. It is accordingly results in the elongated aligned pore channels and short arms channel in the sintered body, as shown in Fig. 13(c).

In the center of the cast body, some of the dendrite side arms might be melted off and then act as seeds for new dendrites, resulting in the formation of equiaxed pore structures (shown in Fig. 13(d)). This unique pore structure in the center of the cast body might be related to the breakaway of the side arms from the primary dendrite of the camphene.

### 3.4 Effect of initial solid loading

Solid loading plays an important role in determining the porosity and mechanical strength characteristics of the sintered samples. Fig. 14(a)–(c) shows the pore structures after sintering at 1500 °C with the solid loading varying from 10 to 20 vol.%. It is clear that lower solid loading results in higher porosity and larger pore sizes, while the sintered zirconia walls became thinner. During freezing, the camphene dendrites can grow until the force created by the particle concentration exceeds the capillary drag force pushing the particles with the solid/liquid interface (Yoon, B. H et al, 2008). Therefore, it is reasonable to suppose that a lower solid loading will lead to the formation of larger camphene dendrites and thinner concentrated $ZrO_2$ ceramic walls.

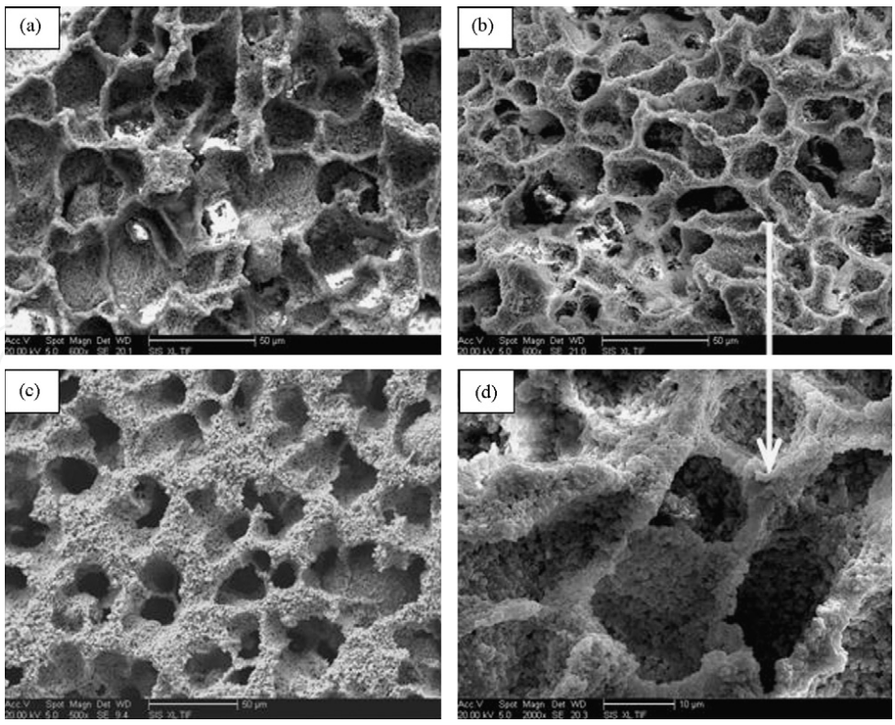


Fig. 14. SEM micrographs of porous structures sintered at 1450 ◦C for (a) 10 vol.%, (b) 15 vol.%, (c) 20 vol.%, and (d) sintered ceramic wall in solid loading of 15 vol.%.

Fig. 15 shows the relationship between the porosity and the initial solid loading of the ceramic slurry. As the solid loading is increased, the porosity was found to decrease proportionately. The porosity was reduced from 81.5 to 65.5% by increasing the solid loading from 10 to 20 vol.%. The linear relationship between the porosity and the initial solid content can be expressed as follows:

$$P = 97.5 - 1.6x \quad (2)$$

where *P* is the porosity (vol.%) and *x* is the solid loading (vol.%).

This result suggests that the porosity can be manipulated by empirically controlling the initial solid loading used in the ceramic/camphene slurry. It should be noted that the possible sublimation of the molten camphene during ball-milling the freeze-casting is not considered in the above equation. From these observations, it is obvious that the camphene-based freeze casting is very useful for producing high porous ceramics with porosities and completely interconnected pore channels, as well as well sintered $ZrO_2$ walls.

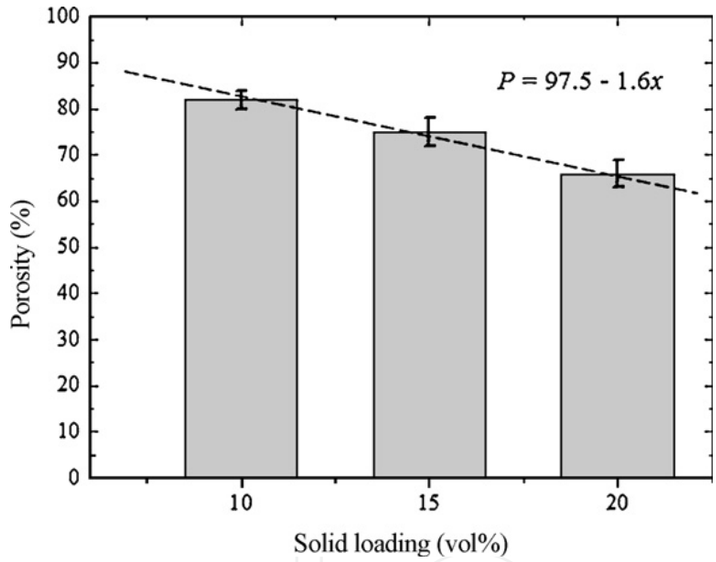


Fig. 15. Relationship between the porosity and the initial solid loading

The main physical and mechanical properties of the sintered samples are summarized in Table 1. The results show that after being sintered with a lower solid content, the sample acquired from 10 vol.% slurry was so light that bulk densities were even lower than water (1.0 g/cm$^3$). As the initial solid loading was increased, the compression strength increased from 16.2 to 53.4MPa.

| Slurry solid loading (vol.%) | Bulk density after sintering(g/cm$^3$) | Compressive strength(MPa) | Porosity content |
|---|---|---|---|
| 10 | 0.93-0.96 | 16.2 | 81.5% |
| 15 | 1.20-1.29 | 32.9 | 74.4% |
| 20 | 1.68-1.69 | 53.4 | 65.5% |

Table 1. Properties of $ZrO_2$ with different initial densities after sintered at 1500 °C for 2 h

Fig. 16 shows the stress–strain curves for 10, 15 and 20 vol.% $ZrO_2$ solid content sintered at 1500 °C. All curves shown almost elastic deformation followed by a transition or plateau stage. No sudden drops or catastrophic fracture are observed, although load drops are found after showing a peak load. Generally, the strength of a porous ceramic is strongly affected not only by the porosity, but also by the formation of sintering neck on the ceramic wall as well as the smaller pore size (several tens of microns) compared conventional processing methods (>100μm). In this observation, pore size was determined by measuring the average size of pores from the SEM micrographs taken at several points on the polished surface. For example, for the 10 and 15 vol.% $ZrO_2$ solid content sintered at 1500 °C, the pore sizes of the prepared sampled approximately ranged from 15 to 30 μm(Fig. 17(a) and (b)). Furthermore remarkable sintering necks were formed (shown in Fig. 17(d)), resulting in high mechanical properties.

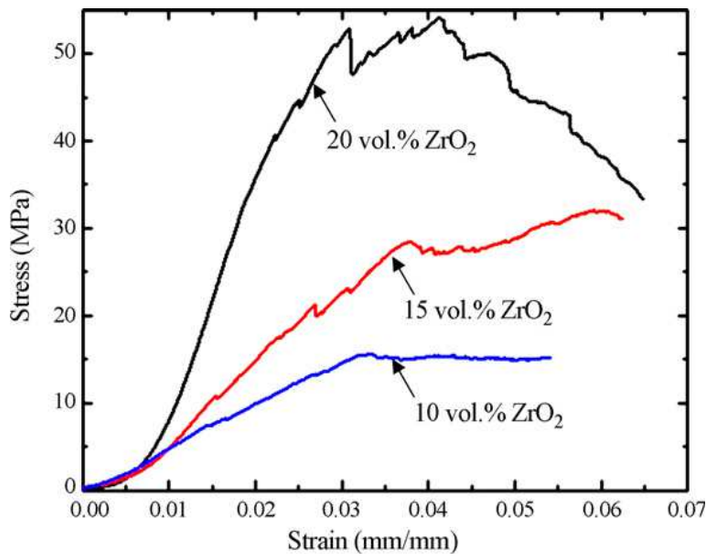


Fig. 16. The stress–strain curves for 10, 15 and 20 vol.% $ZrO_2$ solid content sintered at 1500 °C.

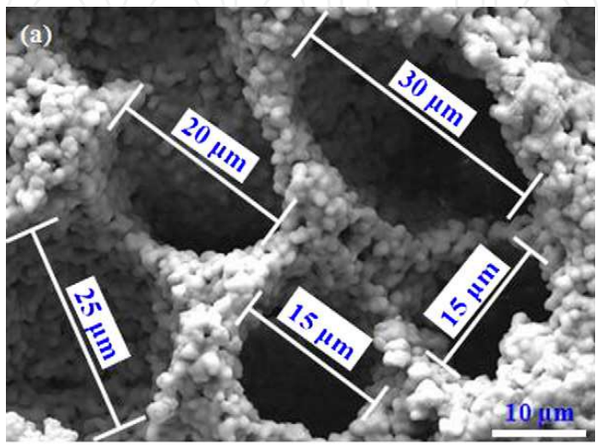

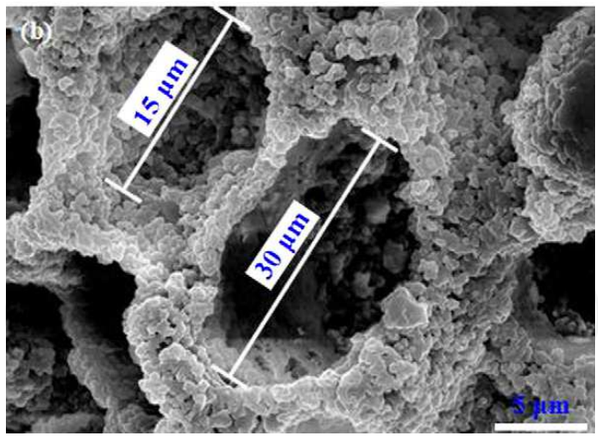


Fig. 17. The pore sizes of the prepared sampled approximately ranged from 15 to 30 µm for the 10 and 15 vol.% ZrO2 solid content sintered at 1500 °C

### 3.5 Effect of sintering temperature

The evolution of microstructure sintered at elevated temperatures ranging from 1400 to 1550 °C is shown in Fig. 18(a)–(d). It can be concluded that with a given initial solid loading (15 vol.%), the sintering temperature significantly contributes to the change of ceramic struts and porosity. As the sintering temperature is increased, the $ZrO_2$ ceramic struts are greatly densified (i.e., loosely bonded particles are observed from Fig. 18(a), while the sintering struts are greatly enhanced in view of Fig. 18(d)).

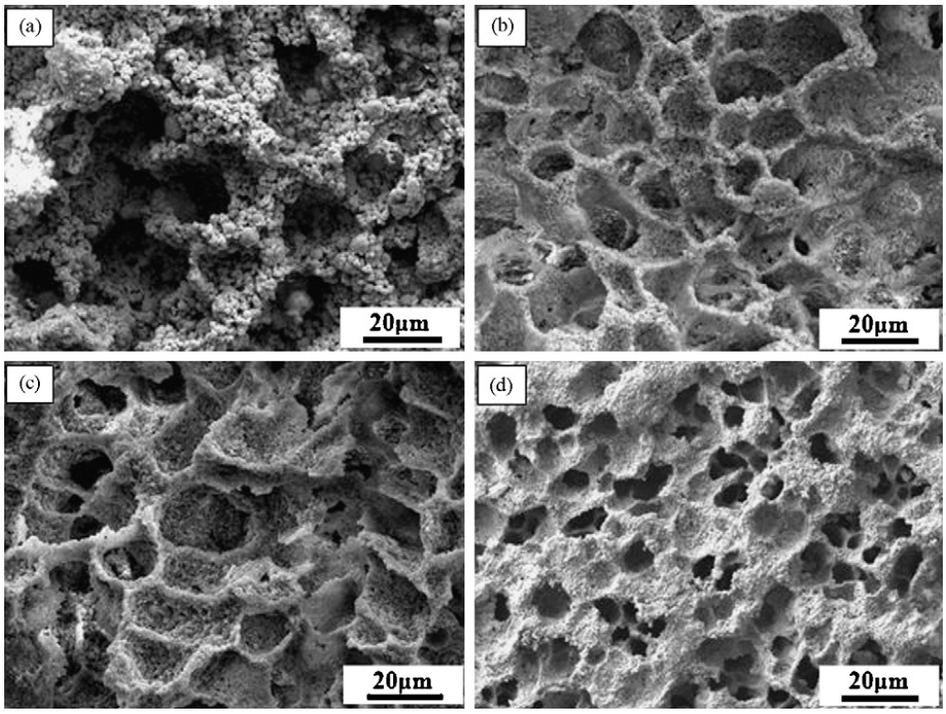


Fig. 18. Scanning electron micrographs of the samples sintered for 2 h in air at (a) 1400 ◦C, (b) 1450 °C, (c) 1500 °C and (d) 1550 °C in solid loading of 15 vol.%.

The effect of sintering temperature on the porosity was also investigated, and the results are shown in Fig. 19. The experimental examinations (as shownin Fig. 19) revealed that the porosity decreases and compressive strength goes up when sintering temperature increases from 1400 to 1550 °C (i.e., 18–59MPa for compressive strength). Both then reach a comparable plateau value, which means that densification is achieved at 1500 or 1550 °C. Further increase in sintering temperature will deteriorate the pore structure. Therefore, the optimum sintering temperature was determined to be 1500 °C in this work. Here, it is worth noting the increasing of $ZrO_2$ grain size with temperature variation is very limited from the experimental observation (see Fig. 18(a)–(d)).

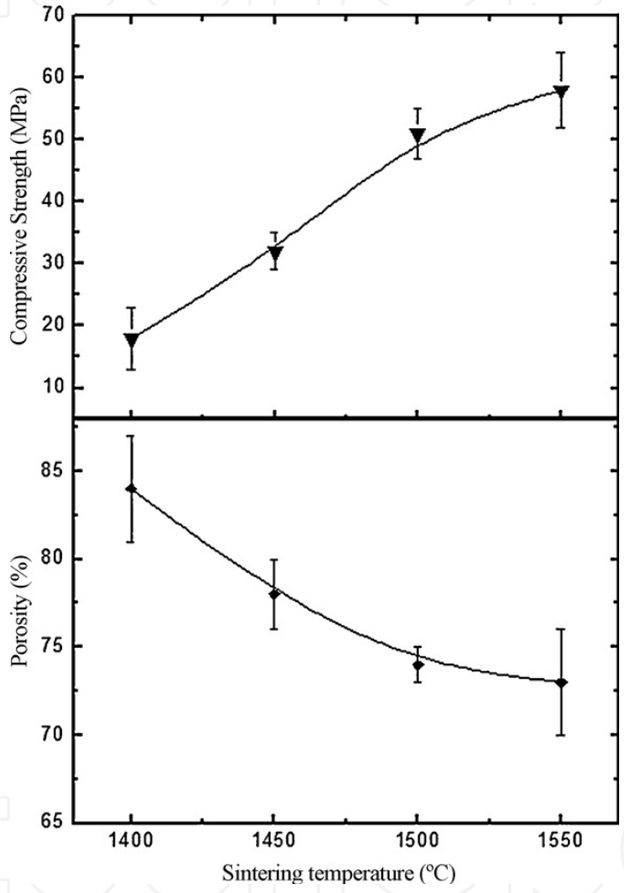


Fig. 19. Influence of sintering temperature (2 h at dwell temperature) on compressive strength and total porosity

Although the proper reasons of this particular phenomenon are still to be explored, it is probably partly related to the pinning of grain boundary at the surface during sintering of thin films, when the grain size lies in the same range of order as the lamellate thickness. Highly porous ceramics fabricated by conventional methods often contain defects, such as cracking and surface flaws. For example, reticulated porous ceramics produced using the polymer replication method have longitudinal cracks and surface flaws on the sintered ceramics struts during pyrolysis of the polymeric sponge. Cellular structures prepared by direct foaming usually exhibit mechanical strengths higher than that of replica techniques

due mainly to the absence of flaws in the cell struts, the sintered foams show moderate compressive strengths of upto 16MPa in alumina foams with porosities of 88% produced from particle-stabilized foams.

Using camphene as the solvent, dilute $ZrO_2$ slurries were produced and large shrinkage during drying was avoided. By adjusting the initial solid loading and sintering temperatures, light-weight $ZrO_2$ ceramics with controlled microstructures and properties were prepared. It was possible to increase the porosity from 65.5 to 84.5%, while still obtaining high mechanical strength (over 16MPa). In addition, the prepared samples produced using camphene as solvent showed well-constructed zirconia walls without any noticeable defects, which might enable them to have good mechanical properties.

## 4. Summary and future perspectives

This chapter introduces pressureless sintering and novel freeze-casting methods are nowadays available for the production of porous ceramics.

Although the two techniques differ greatly in terms of processing features and final microstructures/properties achieved, they have their own merits for producing high-strength ceramics for actual application with special purposes. The pressureless sintering technique is an easy and well-established method to prepare high-strength structures with porosity between 40%and 80%. The freeze-casting based on the novel camphene-based freezing route is a good method for preparing high-porosity ceramic (60-85%) with special microstructure.

For porous $TiB_2$ discussed here, the microstructure of the compacts prepared at lower pressures and lower sintering temperature appeared to decrease the relative density and degrade the interface bonding strength of the $TiB_2$ grain boundaries. The high mechanical properties are related to the enhanced neck growth by surface diffusion at high temperature. Initial solid loading played an important role in the resulting porosity of the materials.

For freeze-casting porous $ZrO_2$ ceramics, the porosity was reduced from 81.5 to 65.5% by increasing the solid loading from 10 to 20 vol.%. As a result of this, the compressive strength was affected, increasing from 16.2 to 53.4MPa for the respective increase in solid loading. The rate of heat transfer affected the final morphology of the dendrites; camphene dendrites were found to orient according to the direction of freezing under liquid nitrogen environment; the sintering temperature (from 1400 to 1550 °C) also affected the porosity and mechanical properties. The porosity (for 15 vol.% solid content) ranged from 73.5 to 84.5 vol.%, while the compressive strength increased from 18 to 59MPa, respectively.

In conclusion, this manufacturing technique shows great potential for generating defect-free porous ceramics with controlled porosity and pore size and appropriate compressive properties for use in modern engineering applications.

## 5. Conclusion

This chapter provides a comprehensive introduction of the synthesis, structure, mechanical properties and characterization of high-strength porous ceramics. It introduces pressureless

sintering and novel freeze-casting methods for the production of porous $TiB_2$ and $ZrO_2$ ceramics. Taking into account the decisive influence of the processing method on the material's microstructure and properties, the selection of the processing route for the production of porous ceramics depends primarily on the final properties and application aimed. For freeze-casting method, this manufacturing technique shows great potential for producing highly porous ceramics with controlled porosity and pore size for use in special engineering applications.

## 6. References


Amir, M. and Rohwer, K(2007). Proc. IMechE, Part G: J. Aerospace Engineering, Vol. 221, 831–845.

Araki, K. and Halloran, J. W(2005). J. Am. Ceram. Soc.Vol. 88, 1108–1114.

Bhaumik, S. K., Divakar, C., Singh, A. K., and Upadhyaya, G. S(2000). Mater. Sci. Eng. A. Vol.279, 275–281.

Cadirli, E., Marasli, N., Bayender, B. and Gunduz, M(2000). Mater. Res. Bull. Vol.35, 985–995.

Chen, R. F., Huang, Y., Wang, C. A. and Qi, J. Q.(2007). J. Am. Ceram.Soc. Vol.90, 3424–3429.

Corbin, S. F. and Apte, P. S. (1999). J. Am. Ceram. Soc., Vol. 82, 1693–1701.

Dale, H. and David, J. G(1995). J. Eur. Ceram. Soc. Vol. 15, 769–775.

Deng, Z. Y., Fukasawa, T., Ando, M., Zhang, G. J., and Ohji, T(2001). Acta Mater. Vol. 49, 1939–1946.

Deng, Z.-Y., Yang, J.-F., and Beppu, Y(2002). J. Am. Ceram. Soc. Vol. 85, 1961–1965.

Deville, S.(2008) Adv. Eng. Mater. Vol.10, 155–169.

Deville, S., Saiz, E. and Tomsia, A. P.(2006) Biomaterials. Vol.27, 5480–5489.

Deville, S., Saiz, E., Nalla, R. K. and Tomsia, A(2006). Science,Vol.311, 515–518.

Fukasawa, T., Ando, M., Ohji, T., and Kanzaki, S(2001). J. Am. Ceram. Soc. Vol.84, 230–232.

Gonzenbach, U. T., Studart, A. R., Tervoort, E. and Gauckler, L. J(2006). J. Am. Ceram. Soc. Vol.90, 16–22.

Gough, J. E., Clupper, D. C. and Hench, L. L(2004)J. Biomed. Mater. Res.Vol.69, 621–628.

Hong, C. Q., Han, J. C., Zhang, X. H., and Meng, S. H.(2007). Mater. Sci. Eng. A, Vol.447, 95–98.

Kamal, M. M. and Monhamad, A. A(2006). Proc. IMechE, Part A: J. Power and Energy, Vol. 220, 487–508.

Kiyoshi, A. and John, W. H.(2004). J. Am. Ceram. Soc.Vol. 87, 1859–1863.

Koh, Y. H., Lee, E. J., Yoon, B. H., Song, J. H. and Kim, H. E(2006). J. Am. Ceram. Soc. Vol. 89, 3646–3653.

Oh, S. T.,Tajima, K. I., Ando, M., and Ohji,T(2000). J. Am. Ceram. Soc., 2Vol. 83, 1314–1316.

Oh, S.-T., Tajima, K.-I., Ando, M., and Ohji, T(2001). Mater. Lett. Vol. 48, 215–218.

Peng, H. X., Fan, Z., Evans, J. R. G., and Busfield, J. J. C(2000). J. Eur. Ceram. Soc., Vol.20, 807–813.

Rice, R. W(1993) .Mater. Sci. Vol. 28, 2178–2190.

Schmidt, H., Koch, D. and Grathwohl, G.(2001) J. Am. Ceram. Soc.Vol. 84, 2252–2255.

She, J. H., Yang, J.-F., and Kondo, N. (2002) J. Am. Ceram. Soc. Vol. 85, 2852–2854.

Studart, A. R., Gonzenbach, U. T., Tervoort, E. and Gauckler, L. J(2006). J. Am. Ceram. Soc. Vol. 89, 1771–1789

Wang, J. H., Gan, M., and Shi, J. X(2007). Mater. Charact. Vol.58, 8–12.

Wang,W. M. and Fu, Z. Y. (2002)J. Eur. Ceram. Soc. Vol.22, 1045–1049.
Waschkies, T., Oberacker, R. and Hoffmann, M. J(2009). J. Am. Ceram. Soc.Vol.92, S79–S84.
Yoon, B. H., Choi, W. Y., Kim, H. E., Kim, J. H. and Koh, Y. H.(2008) Scripta Mater.Vol.58, 537–540.

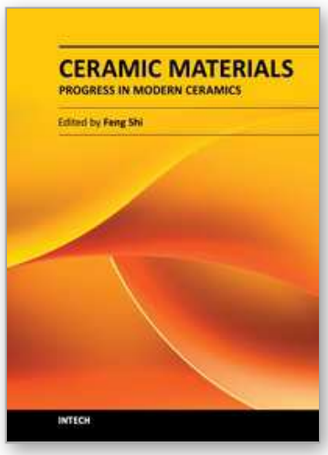


**Ceramic Materials - Progress in Modern Ceramics**

Edited by Prof. Feng Shi

ISBN 978-953-51-0476-6
Hard cover, 228 pages
**Publisher** InTech
**Published online** 05, April, 2012
**Published in print edition** April, 2012

This text covers ceramic materials from the fundamentals to industrial applications. This includes their impact on the modern technologies, including nano-ceramic, ceramic matrix composites, nanostructured ceramic membranes, porous ceramics, and the sintering theory model of modern ceramics.



**InTech Europe**
University Campus STeP Ri
Slavka Krautzeka 83/A
51000 Rijeka, Croatia
Phone: +385 (51) 770 447
Fax: +385 (51) 686 166
www.intechopen.com

**InTech China**
Unit 405, Office Block, Hotel Equatorial Shanghai
No.65, Yan An Road (West), Shanghai, 200040, China
中国上海市延安西路65号上海国际贵都大饭店办公楼405单元
Phone: +86-21-62489820
Fax: +86-21-62489821

IntechOpen